



Advanced green capture of microplastics from different water matrices by surface-modified magnetic nanoparticles

Daniel Aragón, Belén García-Merino, Carmen Barquín, Eugenio Bringas^{*}, Maria J. Rivero, Inmaculada Ortiz

Departamento de Ingenierías Química y Biomolecular, ETSIT, Universidad de Cantabria, Avda. Los Castros s/n, Santander 39005, Spain

ARTICLE INFO

Keywords:

Magnetic nanoparticles
Amino-functionalization
SA-functionalization
Polyethylene microplastics (PE MPs)
Capture

ABSTRACT

The extensive production and application of plastic in recent decades has resulted in the presence of microplastics (MPs) in different water bodies. Considered as contaminants of emerging concern (CECs), MPs are accessible to a wide range of organisms and can act as vectors for the transport of other persistent organic pollutants. The existing technologies to remove microplastics from wastewaters and prevent their intrusion in nature, still present several limitations, resulting in an urgent need to develop novel, fast, cost-effective and greener alternatives. In this work, the magnetophoretic capture of MPs by their assembly with magnetic nanoparticles through either electrostatic interactions or molecular forces is investigated. For the experimental assessment, magnetic nanoparticles were synthesized by hydrothermal coprecipitation and solvothermal decomposition methods, while polyethylene (PE) microspheres were selected as model microplastic pollutants. As a noteworthy novelty, thermal decomposition and coprecipitation particles were functionalized with amino groups and sodium alginate (SA), respectively, resulting in a modification of their surface properties and enhanced electrostatic or molecular interactions with MPs. After preliminary experiments, a concentration of 1.3 g L^{-1} and a contact time of 20 min between magnetic nanoparticles and MPs, were selected as operating conditions to assess the influence of the functional groups on the capture performance. The influence of other variables in the process was also evaluated, including the magnetic nanoparticles synthesis method, the pH of the medium, varied in the range 4–8, and the water constituents that may be present in water bodies. Results demonstrated that the presence of different types of polar groups on the surface of the magnetic nanoparticles make them interact towards MPs through electrostatic attraction or molecular forces, considerably enhancing the capture performance of bare magnetic nanoparticles. This work represents a step forward in the development of new and reliable techniques for the environmentally friendly capture of microplastics from polluted waters.

1. Introduction

During the last decades, plastics have been broadly applied in a wide range of daily life products, such as clothing, personal care items or packaging, among others. This extensive use has resulted in a large-scale production, up to 400.3 million tonnes in 2022, and to the release of significant amounts of plastic waste into the environment, over 14 million tons in oceans annually [1,2]. After weathering and ultraviolet radiation, larger plastic debris break down into smaller pieces [3]. Specially, microplastics (MPs) are plastic particles with dimensions lower than 5 mm that can be made of different polymers and come in a variety of forms, including spheres, fragments, and fibers [4]. They are emerging pollutants which have been found in oceans, rivers,

groundwater, wastewater, air and soil, where they can last for hundreds to thousands of years. Several studies have identified the presence of these pollutants in the environment with concentrations of $70.8 \text{ particles m}^{-3}$ in the Northeast Atlantic Ocean [5] and ranging from 0.28 to 4.18 MPs L^{-1} in secondary effluents of wastewater treatment plants depending on the treatments carried out [6]. According to their formation, they are classified into primary and secondary microplastics. Primary MPs are intentionally produced by industry, for their addition into final products to enhance specific properties, for example in personal care and household products; while secondary microplastics result from the degradation of larger plastic debris by solar radiation, wave action, temperature change or other physical, chemical, and biological effects [1,7]. Due to their small size, MPs are accessible to a wide range

^{*} Corresponding author.

E-mail address: bringase@unican.es (E. Bringas).

<https://doi.org/10.1016/j.seppur.2024.128813>

Received 16 May 2024; Received in revised form 25 June 2024; Accepted 12 July 2024

Available online 19 July 2024

1383-5866/© 2024 The Author(s). Published by Elsevier B.V. This is an open access article under the CC BY-NC license (<http://creativecommons.org/licenses/by-nc/4.0/>).

of organisms including the marine biota and humans. In addition, due to their hydrophobicity and relatively high specific surface area, they have a high capacity to adsorb other contaminants, providing a vector for the transport of persistent organic pollutants [8–12]. Because of their high accumulation in the environment and potential hazardous effects, there is an urgent need to find methods for the removal of MPs. However, only a very limited number of studies have been reported on their removal from aqueous media, most of which have been published in recent years.

The most widely used technology for MPs removal is sedimentation facilitated by coagulants and flocculants, with remarkable removal efficiencies around 95% [13,14]. Even though it is easy to handle and has the capacity to capture small MPs, this technique presents several limitations related to the long time required and to the high consumption of reactants, which significantly increase the operating costs and may lead to excessive levels of coagulants and flocculants in the effluent [15]. In addition, floc formation is strongly influenced by the characteristics of the aqueous media including the pH, organic matter content and coexisting anions, among others [16]. Another reported technology is filtration using membranes with a specific pore size. It is easy to handle and to scale-up and shows high removal efficiencies with low energy requirements [17]. Kim et al. [18] demonstrated high efficiency in the removal of MPs from simulated laundry water, capturing 99.88%, using ceramic membranes. However, its bottleneck is the fouling phenomenon that membranes usually suffer due to accumulation of the MPs in the pores, giving place to their clogging, considerably reducing their removal capability and lifetime, and increasing costs related with their maintenance. Bioremediation is a technology that involves the use of different microorganisms to degrade microplastics. It is easy to handle, cost-effective, environmentally friendly and presents high removal efficiencies, between 50 and 98% depending on the bioreactor [19]. Moreover, microorganisms can adapt to the different environmental conditions presented by the aqueous media [20]. Nonetheless, it also presents some drawbacks, especially the long degradation times, the inability to reuse microorganisms and the difficult scale-up. Furthermore, the use of both membranes and microorganisms can lead to the generation of secondary microplastics [21]. Advanced oxidation processes are environmentally friendly technologies that are attracting attention for their ability to degrade MPs in a short time. However, to date, they have low removal efficiency with a 3% weight loss and can result in the formation of by-products [22,23].

Adsorption is a methodology that has been previously proved with many other pollutants. It overcomes most of the limitations of the previously reported techniques, as it shows high removal efficiency within relatively short operation times, and it does not imply high energy costs, reactants consumption or complex processes [24]. However, the adsorbents that have been reported until date for the capture of MPs, including carbonaceous materials, zeolites, polymers, and inorganic clays, usually present a rapid saturation and high costs related with the regeneration step [20,22]. Microplastics are generally characterized by a strong hydrophobicity, thus presenting affinity towards other highly hydrophobic materials [25,26]. Besides, the pH of the water matrix plays an important role, as it can modify the superficial charges of both microplastics and adsorbent particles, modifying the electrostatic interactions between them [27]. Microplastics usually present isoelectric points around pH 4, which means that at higher pH values, MP's surface is negatively charged and presents electrostatic attractions towards positively charged particles [28,29]. As an alternative, this work proposes the use of the adhesion of functionalized magnetic nanoparticles on the surface of microplastics to remove these pollutants from wastewaters. This alternative takes advantage of the characteristics of magnetic nanoparticles, such as high surface area which favours the interaction with target compounds; physical and chemical stability; high mobility, resulting in short diffusion distances, fast kinetics, and thus in reduced costs and improved efficiency [30]. Moreover, the functionalization provides remarkable advantages to enhance the possibility of diverse type of interactions. The main mechanisms for magnetic

nanoparticles adhesion on microplastics include electrostatic interactions and molecular forces. With the aim of removing microplastics from polluted water, functionalized magnetic nanoparticles offer a sustainable solution. These particles exhibit high adhesive capacity and superparamagnetic behaviour below a certain diameter, which is material-dependent, allowing the facilitated recovery of loaded nanoparticles under the action of a magnetic field [31–33]; and finally, the possibility to be regenerated in a short time by modifying the surface tension with the aid of surfactants or by adjusting the surface charge after saturation via pH value in a cost-effective process [34–37].

So far, there are very few works that study the applicability of magnetic nanoparticles for the capture of microplastics. In 2020, Grbic et al. [38] obtained hydrophobic nanoparticles by functionalizing commercial Fe magnetic nanoparticles with silane; more than 92% of MPs with size < 20 µm and > 1000 µm were recovered from seawater, while 78% and 84% of 200–1000 µm MPs were separated from freshwaters and sediments, respectively. Misra et al. [39] synthesized hydrophobic core-shell iron oxide/silica particles following a microemulsion method and coating them with an ionic liquid; 100% removal was reported for 1 µm and 10 µm polystyrene beads after 24 h of contact time. Shi et al. [40] used commercial Fe₃O₄ nanoparticles and a contact time of 150 min, to obtain average removal percentages of 87%, 85%, 86% and 63% for the capture of 200–900 µm polyethylene, polypropylene, polystyrene and polyethylene microplastics, respectively. Bhole et al. [41] functionalized commercial iron oxide (II-III) nanoparticles (50–150 nm) with phosphotungstic acid and different amines leading removal percentages of 1 µm polystyrene microplastics higher than 99%. Lastly, Martin et al. [42] synthesized magnetic nanoparticles following a thermal decomposition method and coated them with hydrophobic polydimethylsiloxane, reporting recoveries of nearly 90% for microplastics with size in the range 2–5 mm and 100% captures for 100–1000 nm MPs. Therefore, it is important to design magnetic nanoparticles in order to reduce the operation time and to address the optimum working conditions leading to different superficial properties that can drive the MPs capture by different mechanisms.

In this study, magnetic nanoparticles were synthesized using two synthesis methods: the hydrothermal method of coprecipitation and the solvothermal method of thermal decomposition, whose main difference lies in the coating that is formed on the thermal decomposition particles due to the surfactant employed during the synthesis [43]. Then the particles synthesized by both methods were compared in terms of their properties such as composition, superficial charge, size, and on their performance for the capture of microplastics. Different initial concentrations of the synthesized magnetic nanoparticles and contact times were applied to study the capture of polyethylene (PE), selected as a model target pollutant. As previously mentioned, the global plastic production raised up to 400.3 million tonnes in 2022, being polyethylene plastics the predominant ones, accounting for a 26.3% of the total plastic produced [2]. Furthermore, several studies reported the presence of these microplastics in oceans and secondary effluents of wastewater treatment plants [44–46]. As a remarkable novelty, different functionalization processes were employed to enable a new insight into the interactions between PE MPs and different surface-modified magnetic nanoparticles for the removal of these contaminants of emerging concern from water matrices. Amino groups were grafted on the surface of thermal decomposition particles with the aim of modifying their superficial charge and isoelectric point, increasing the pH range at which they present electrostatic attractions towards negatively charged MPs. Moreover, a cost-effective and greener functionalization process with sodium alginate was applied to the coprecipitation particles to evaluate if the mechanism based on hydrogen bonding, instead of electrostatic attraction could lead to a faster MPs capture. Sodium alginate is a biodegradable, renewable and biocompatible material which has a large number of industrial applications in many fields such as biotechnology, biomedicine and food industries [47]. In summary, the results reported in this work shed light on the capture mechanism of PE MPs using

functionalized magnetic nanoparticles and contribute to the development of new reliable techniques for the fast, cost-effective and environmentally friendly separation of microplastics from different polluted water sources.

2. Materials and methods

2.1. Materials

Triethylene glycol (TEG, $C_6H_{14}O_4$) and ethyl acetate ($C_4H_8O_2$, 99.9%) were purchased by Fisher Chemical (Madrid, Spain). Iron (III) acetylacetonate ($Fe(acac)_3$, 97%), ferrous chloride ($FeCl_2 \cdot 4H_2O$, $\geq 99\%$), ferric chloride ($FeCl_3 \cdot 6H_2O$, $\geq 99\%$), n-[3-(trimethoxysilyl)propyl] ethylenediamine (TMPEd, 99%), sodium hydroxide (NaOH 2 M), hydrochloric acid (HCl, 2 M), ammonia (NH_3 , 30%) and sodium alginate ($(C_6H_7NaO_6)_n$) were obtained from Sigma-Aldrich (Buchs, Switzerland). Toluene dry ($C_6H_5CH_3$, 99%) and isopropyl alcohol (C_3H_8O , 99.5%) were supplied by PanReac AppliChem (Barcelona, Spain), and ethanol (C_2H_5OH , $\geq 99.5\%$) was purchased by Merck (Darmstadt, Germany). All chemicals were used as received without further purification and solutions were prepared with ultrapure water (18 M Ω · cm Millipore), tap water, natural Cantabrian Sea water and WWTP secondary effluent. Wastewater samples were collected from the secondary effluent of Vuelta Ostrera Wastewater Treatment Plant (WWTP) (Cantabria, Spain) and stored in amber bottles in the dark at 4 °C. Besides, the characterization of the different water bodies employed is shown in Table S1. Fluorescent green polyethylene microspheres with a size of $231 \pm 19 \mu m$ were provided by Cospheric (California, United States).

2.2. Synthesis and functionalization of magnetic nanoparticles

Two different methods were used for the synthesis of magnetite nanoparticles: thermal decomposition and coprecipitation. Then, the surface of the magnetic nanoparticles synthesized by thermal decomposition was functionalized with primary and secondary amino groups by means of the alkoxy silane TMPEd in order to evaluate the role of electrostatic interactions with MPs. Besides, the magnetic nanoparticles synthesized by coprecipitation were coated by sodium alginate (SA) to analyze the importance of molecular forces in their interaction with MPs. Both the synthesis and amino-functionalization steps of thermal decomposition particles are based on protocols reported in a previous work of the research group [34]. Moreover, the synthesis and SA-functionalization of coprecipitation particles are based on the works reported by Molaei and Salimi [48] and El-Shamy et al. [49].

Briefly, for the thermal decomposition synthesis, 2.1 g of $Fe(acac)_3$ were suspended in 75 mL of TEG, sonicated for 5 min (FB 15050, Fisher Scientific) and poured into a three-necked round bottom flask equipped with a heating mantle, magnetic stirrer, condenser, and inert nitrogen atmosphere. The mixture was heated at 180 °C for 30 min and then, at 280 °C for further 30 min. The resulting suspension was cooled down to room temperature and centrifuged (Eppendorf 5810, 10000 rpm). The particles were then separated using a magnet, washed three times with 30 mL of ethanol and 60 mL of ethyl acetate and dried in an oven at 100 °C until completely dry.

For the coprecipitation synthesis, 6.4 g of $FeCl_3 \cdot 6H_2O$ and 2.4 g of $FeCl_2 \cdot 4H_2O$ were added to 200 mL of ultrapure water. This solution was stirred in a three-necked round-bottom flask equipped with a heating mantle, magnetic stirrer, and Ar inlet for 30 min. Then by dropwise addition of NH_3 , pH increased and black precipitates were formed. Then, the resulting suspension was centrifuged and washed several times until reaching neutral pH conditions. The particles were separated using an external magnet and dried in an oven at 80 °C until completely dry.

For the amino-functionalization, 500 mg of thermal decomposition nanoparticles were suspended in 50 mL of toluene and 2 mL of TMPEd.

The mixture was sonicated for 5 min and poured into a three-necked round bottom flask and heated to 110 °C for 3 h with a heating mantle equipped with magnetic stirrer, condenser, and inert nitrogen atmosphere. The resulting suspension was cooled down at room temperature and centrifuged, the particles were separated with the help of a magnet, purified three times with 10 mL of isopropyl alcohol and dried in an oven at 120 °C to remove traces of toluene.

For the SA-functionalization of the coprecipitation particles, 15 g of SA were added to 500 mL of ultrapure water and stirred vigorously until its complete dissolution. Then, the resulting solution was mixed with 800 mg of coprecipitation nanoparticles and stirred for 5 h. After centrifugation, the functionalized nanoparticles were collected with a magnet and dried overnight.

2.3. Characterization of microplastics and magnetic nanoparticles

Several techniques were used to confirm the surface properties of the functionalized magnetic nanoparticles; Fourier-transform infrared (FT-IR) spectroscopy was applied using a Perkin Elmer Spectrum 65 spectrometer acquired from Perkin Elmer (Madrid, Spain); the measurement was carried out in a reflectance spectrum between 400 and 4000 cm^{-1} , with a resolution of 4 cm^{-1} , 150 scans and a step speed of 2 $mm s^{-1}$. Zeta potential values were obtained by means of dynamic light scattering techniques in a Zetasizer Nano ZS equipment provided by Malvern (Worcestershire, United Kingdom); the instrument was calibrated using latex particles as reference material (DTS1235 standard), and all the measurements were triplicated, at room temperature, using 0.1 $mg mL^{-1}$ solutions previously sonicated for 10 min, with 17 °C angle glass cuvettes. The size and shape of the PE MPs were obtained with a stereo microscope (Nikon SMZ18) obtained from Nikon Instruments Inc. (Amstelveen, Netherlands), equipped with a green fluorescence filter (light wavelength $\sim 550 nm$) and a Jenoptik ProgRes C5 camera; images were taken and studied using the ProgRes® CapturePro software (CapturePro V2.10.0.0). The size and shape of the magnetic nanoparticles were determined in a Transmission Electron Microscope (TEM) Jeol JEM 1011 for coprecipitation particles and Jeol JEM 2100 for thermal decomposition particles supplied by JEOL (Benelux, Belgium). The images were analyzed by ImageJ software. Morphological characterization and elemental analysis were obtained by scanning electron microscopy (SEM) and energy dispersive analysis (EDX) using Carl Zeiss, model EVO MA15 microscope acquired from ZEISS (Munich, Germany). The magnetic properties of the nanoparticles were evaluated with a Quantum Design MPMS XL-5 SQUID magnetometer provided by Quantum Design (Grimbergen, Belgium) whilst heating from 2 to 300 K under different applied magnetic fields from 1 to 85 kOe. A thermogravimetric analysis (TGA) was carried out in a TGA/DTA-DTG Shimadzu equipment, heating the sample up to 1000 °C purchased from METTLER TOLEDO (Barcelona, Spain). The dispersion of the magnetic nanoparticles in the different water matrices were employed in an ultrasonic bath (FB15050) with a frequency of 50/60 Hz, a power of 80 W and a voltage of 220–240 V acquired from Fisher Chemical (Madrid, Spain).

2.4. Experimental procedure for the capture of microplastics

When dealing with nanomaterials, several variables must be considered to evaluate the PE MPs capture efficiency such as the concentration and contact time of both MPs and magnetic nanoparticles, the morphology and composition of MPs, the properties of magnetic nanoparticles acquired from different synthesis and functionalization methods, the quality of the water matrix and the experimental capture procedure. To assess the performance of the magnetic nanoparticles on the capture of MPs, a set of experiments was designed to evaluate the influence on the capture efficiency of various mentioned variables: i) the concentration of magnetic nanoparticles; ii) the synthesis method of the magnetic nanoparticles, including thermal decomposition and coprecipitation; iii) the contact time between polyethylene MPs and both types

were analyzed with a stereo microscope equipped with a green fluorescence filter. Moreover, the resulting supernatant was filtered, retained polyethylene MPs were dried in the desiccator and once they were completely dried, the final solid was weighted to calculate the amount of non-captured microplastics. All the experiments were duplicated to check their reproducibility. Therefore, the results obtained are shown as mean values \pm standard deviation. The capture percentage (η , %) was calculated applying Eq. (1) where C_{initial} is the initial concentration of MPs in water and C_{final} is the concentration of non-captured MPs after predetermined time intervals.

$$\text{PE MPs capture(\%)} = \frac{(C_{\text{initial}} - C_{\text{final}})}{C_{\text{initial}}} \cdot 100 \quad (1)$$

3. Results and discussion

3.1. Characterization of microplastics and magnetic nanoparticles

Fig. 2 shows the FT-IR spectra of the polyethylene microspheres, sodium alginate and SA-functionalized and bare coprecipitation particles. Regarding the spectrum of polyethylene MPs, bands in the range of $500\text{--}800\text{ cm}^{-1}$ are attributed to the C–C stretching vibrations, while the band located at around 1000 cm^{-1} is attributed to the coupling of the rocking of CH_2 and CH_3 . Finally, the intense bands at 1460 cm^{-1} and in the range of $2780\text{--}2970\text{ cm}^{-1}$ are assigned to the bending vibration and stretching mode of CH_2 , respectively [50,51]. In the two samples of magnetic nanoparticles, iron oxide is the core material, thus, all the spectra show an intense band at a wavelength around 520 cm^{-1} , corresponding to the Fe–O bond at the octahedral and tetrahedral sites of Fe_3O_4 [52]. The bare coprecipitation particles do not present any other significant band except at 3200 cm^{-1} due to the presence of adsorbed

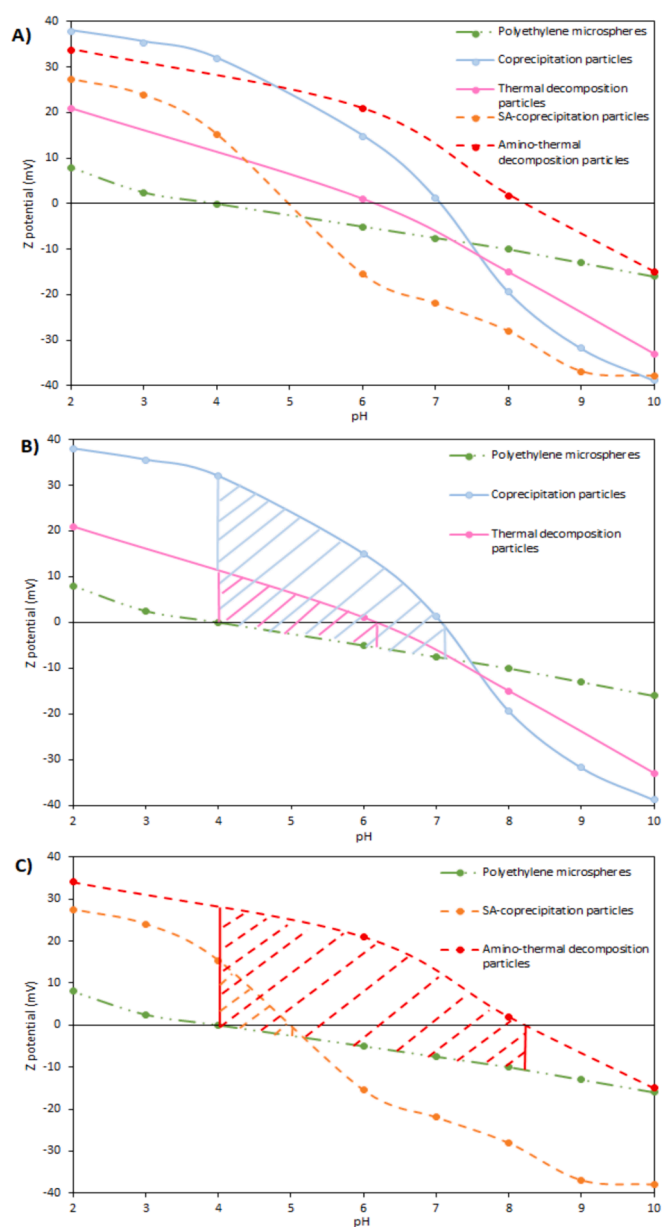


Fig. 3. A) Z potential as a function of pH (pH 2 - pH 10) for the PE microspheres, SA-functionalized and bare coprecipitation particles and amino-functionalized and bare thermal decomposition particles. B) Range of pH at which magnetic nanoparticles could be electrostatically attracted towards PE microspheres and C) Range of pH at which functionalized magnetic nanoparticles could be electrostatically attracted towards PE microspheres.

water [53]. When these particles are functionalized with sodium alginate, some bands corresponding to carboxyl groups appear at 1608 and 1400 cm^{-1} , and 1064 cm^{-1} related to C–O vibrations of carbonyl groups. Furthermore, the SA-functionalized coprecipitation spectra still presents bands at 3200 cm^{-1} and 3640 cm^{-1} related to the hydroxyl groups of the remaining water adsorbed on the particles and the O–H vibrations in the sodium alginate, respectively [48].

Besides, in Fig. 2, the thermal decomposition particles present additional bands compared to the spectra of coprecipitation particles, corresponding to the O–H bending vibration at 1000 cm^{-1} , the O–H stretching vibration at 1550 cm^{-1} and the C–H stretching vibrations at 1300 and 2900 cm^{-1} . The presence of these bands is attributed to the TEG coating that is formed around the magnetic cores during the thermal decomposition synthesis process [34,54–57]. When these particles are amino-functionalized, the FTIR spectrum shows two additional bands at 770 and 1600 cm^{-1} corresponding with the stretching Si–O–Si

vibration of the siloxane groups and to the characteristic bands of the amino groups, respectively [34,56–60].

Fig. 3A displays the zeta potential values as a function of pH (from pH 2 to pH 10) for MPs, bare magnetic nanoparticles and functionalized magnetic nanoparticles. Zeta potential (or Electrokinetic potential) is a measure of the magnitude of the electrostatic repulsion/attraction between particles and is one of the fundamental parameters known to affect stability of dispersed systems. When a material comes in contact with a liquid, the functional groups on its surface react with the surrounding medium. This process results in a surface charge, which attracts the accumulation of oppositely charged ions [61,62]. For all cases, the zeta potential values of the different materials increase while decreasing the pH. As expected, the Z potential values obtained for PE MPs are consistent with those reported in the literature, since they exhibit negative Z potential values at $\text{pH} \geq 4$ [63–65]. On the other hand, all samples of the bare magnetic nanoparticles present a positive

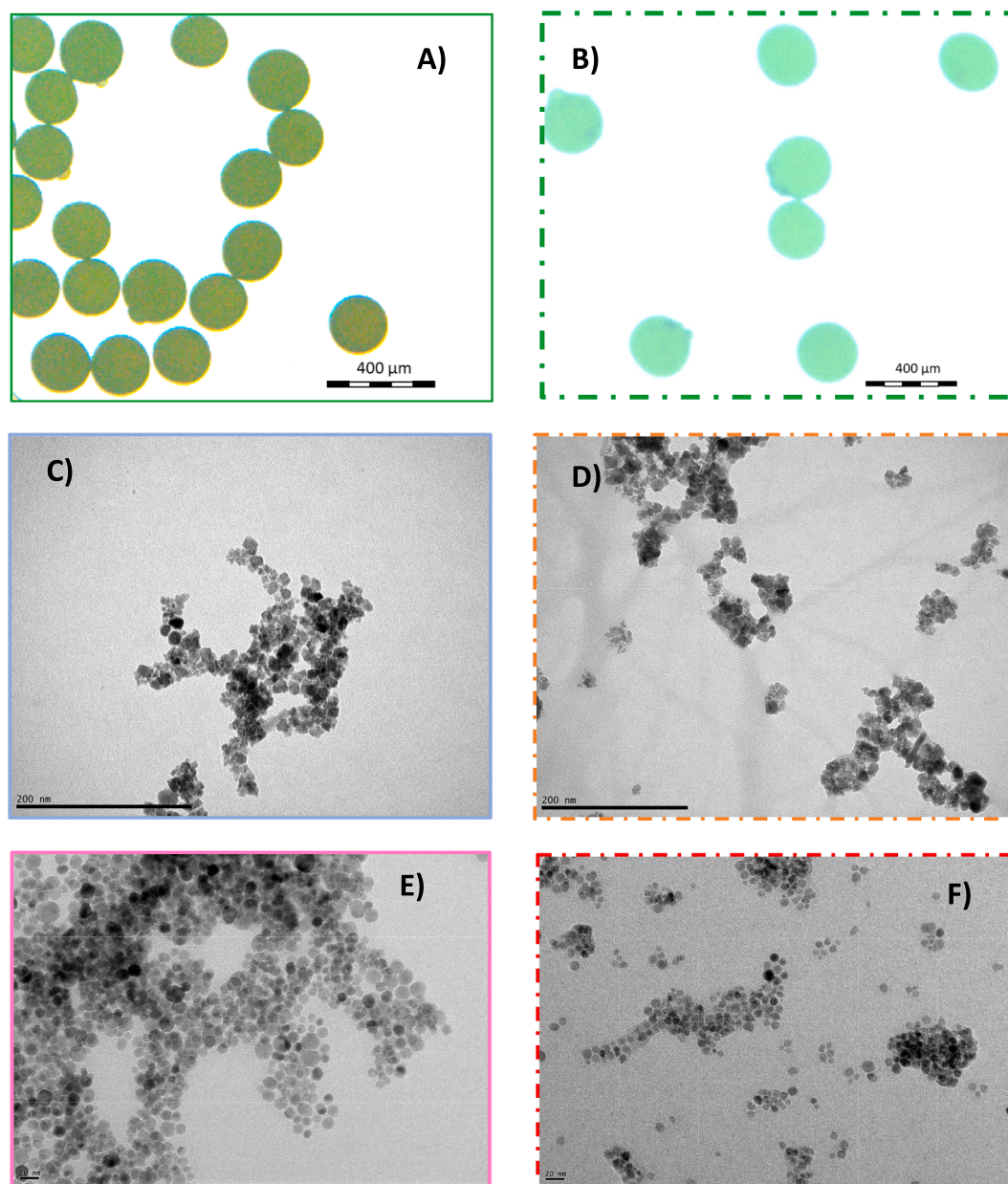


Fig. 4. Optical microscope and TEM images of A) polyethylene microspheres (scale bar $400\text{ }\mu\text{m}$), B) magnetic nanoparticles adhered to polyethylene microspheres (scale bar $400\text{ }\mu\text{m}$), C) bare and D) SA-functionalized coprecipitation particles (scale bar 200 nm), E) bare and F) amino-functionalized thermal decomposition particles (scale bar 20 nm).

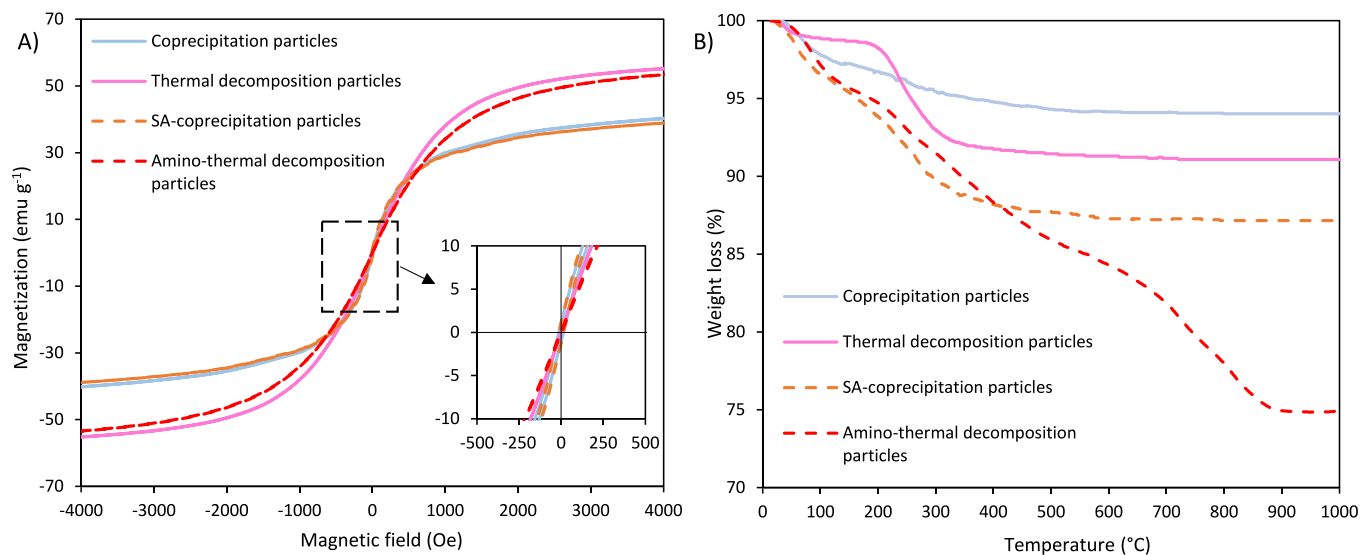


Fig. 5. A) Magnetic hysteresis curves (27° C) and B) thermogravimetric analysis of the SA-functionalized and bare coprecipitation particles and amino-functionalized and bare thermal decomposition magnetic nanoparticles. Magnetization and thermogravimetric curves of amino-functionalized and bare thermal decomposition particles were obtained from a previous work of the research group [34].

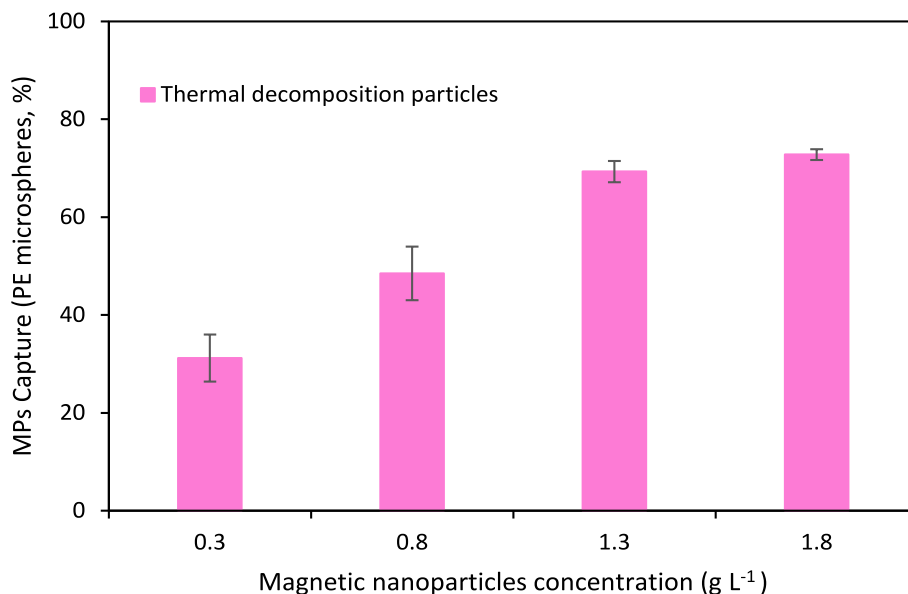


Fig. 6. Percentage of microplastics capture applying different concentrations of thermal decomposition particles. PE microspheres concentration: 0.5 g L⁻¹. Contact time: 20 min. pH: 5.2 ± 0.3.

surface charge for acidic pH values while negative values of Z potential are observed at basic pH values. As previously reported in the literature, non-functionalized magnetic nanoparticles have isoelectric points between pH 6 and 7 [34,58,59,66,67]. Furthermore, surface modification shifts the isoelectric point to higher or lower values depending on the functional groups grafted on the surface. For example, sodium alginate shifts the magnetic nanoparticles curve to lower zeta potential values, while amino groups increase zeta potential values. The comparison of the curves leads to several conclusions: i) after functionalization of the magnetic nanoparticles, zeta potential values vary significantly, confirming the modification of the surface due to the presence of amino groups and sodium alginate; ii) zeta potential values reduce when coprecipitation particles are functionalized with sodium alginate, decreasing the pH range of potential electrostatic attraction; iii) amino-functionalization increases zeta potential values of the thermal decomposition particles and extends the pH range in which the microplastics

and the particles have opposite charge [34,58,59].

Fig. 3B shows the pH range where PE MPs and bare magnetic nanoparticles have opposite surface charge; it is clearly seen that coprecipitation and thermal decomposition particles might present electrostatic affinity to MPs in the range of pH 4–7 and pH 4–6, respectively. The lower isoelectric point of the thermal decomposition particles points to less affinity for polyethylene microspheres compared to the coprecipitation particles due to the narrower pH range where magnetic nanoparticles and MPs exhibit opposite surface charge. The reduced value of the isoelectric point of the thermal decomposition particles is attributed to the organic TEG coating, that is formed around the magnetic core during the synthesis process, which provides hydroxyl groups and reduces zeta potential values [49,68].

As shown in Fig. 3C, amino-functionalization raises the isoelectric point to pH 8, leading the magnetic nanoparticles to have electrostatic affinity towards negatively charged microplastics in the range of pH 4–8.

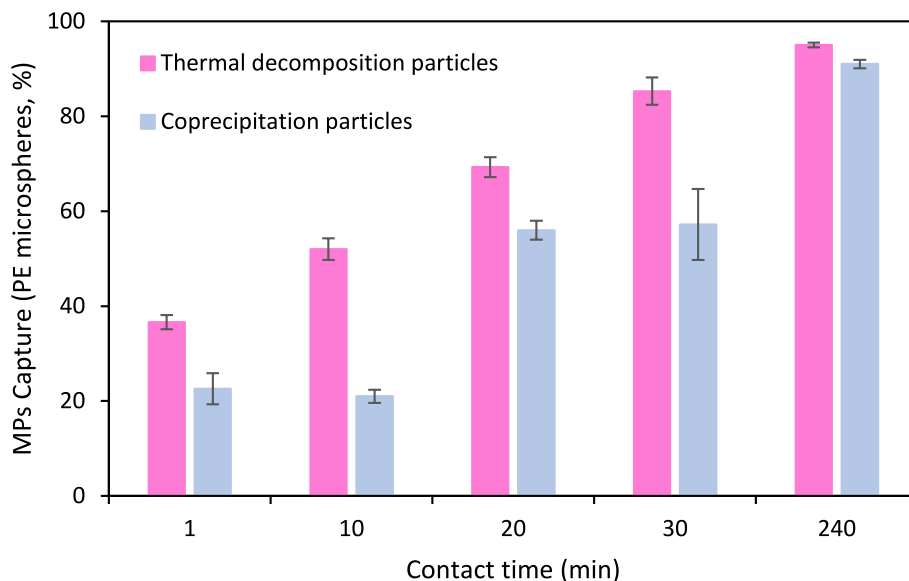


Fig. 7. PE MPs capture percentages applying bare coprecipitation and thermal decomposition particles, with contact times in the range 1–240 min. PE MPs concentration: 0.5 g L^{-1} . Magnetic nanoparticles concentration: 1.3 g L^{-1} . pH: 5.2 ± 0.3 .

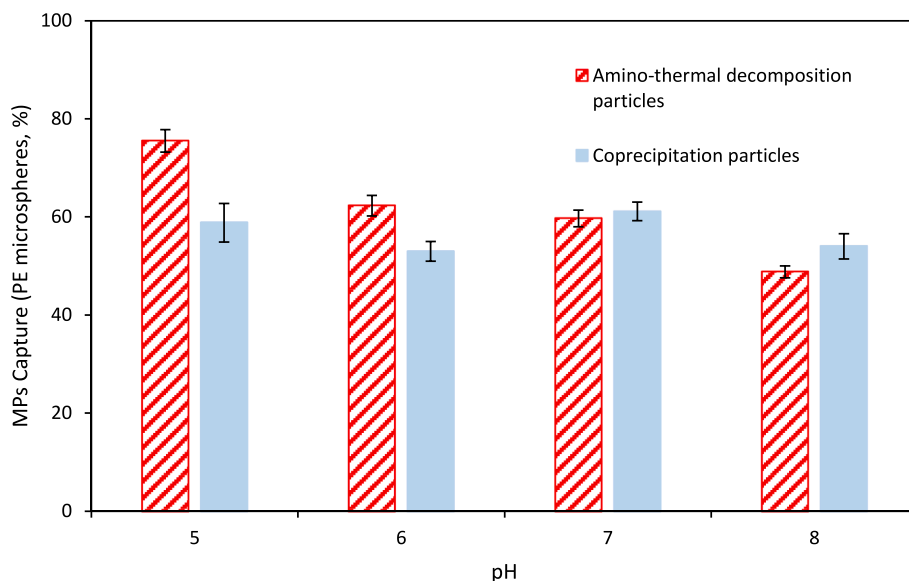


Fig. 8. PE MPs capture percentage applying amino-functionalized thermal decomposition and bare coprecipitation particles, with pH in the range 5–8. PE MPs concentration: 0.5 g L^{-1} . Magnetic nanoparticles concentration: 1.3 g L^{-1} . Contact time: 20 min.

Besides, natural water bodies display pH values ranging from pH 7 to pH 8, which means that there is no need to change this parameter [69–71]. However, SA-functionalized particles have the isoelectric point at pH 5, so magnetic nanoparticles are expected to have electrostatic interactions between pH 4 and pH 5, which is a narrower range, compared to amino-functionalized particles and does not coincide with the natural pH of the effluents. As a result, if electrostatic interactions were the main mechanism responsible for the interactions between magnetic nanoparticles and MPs, amino-functionalized magnetic nanoparticles would be better suited for capturing negatively charged microplastics over a wider pH range than SA-functionalized and bare particles.

Fig. 4 displays the optical microscope image of polyethylene microspheres and magnetic nanoparticles adhered to them, as well as TEM images of SA-functionalized and bare coprecipitation particles, and amino-functionalized and bare thermal decomposition particles. PE microspheres present a mean measured diameter of $232 \pm 8 \mu\text{m}$ with

spherical shape which is consistent with the characteristics reported by the supplier. All magnetic nanoparticles showed spherical shape regardless of the synthesis method. In the case of coprecipitation synthesis, the particles had average diameters of $8.9 \pm 1.2 \text{ nm}$, similar to the value of 8.2 nm reported in previous works of the research group for a similar synthesis procedure [34]. The particles obtained by thermal decomposition reported mean size about $11.7 \pm 1.3 \text{ nm}$, which are similar to the values found in literature following the same synthesis methodology. For instance, Cai and Wan [54] reported a mean diameter of 7 nm ; Maity et al. [55] reported an average diameter of 11 nm and a previous work of the same research group reported a value of 12.1 nm [34]. Differences in size of bare magnetic nanoparticles from different synthesis methods were not significant, possibly attributable to slight variations in the experimental procedure. After SA-functionalization, the diameter of the particles increases to $13.7 \pm 1.0 \text{ nm}$ due to the coating of sodium alginate. Finally, it is observed that the particle

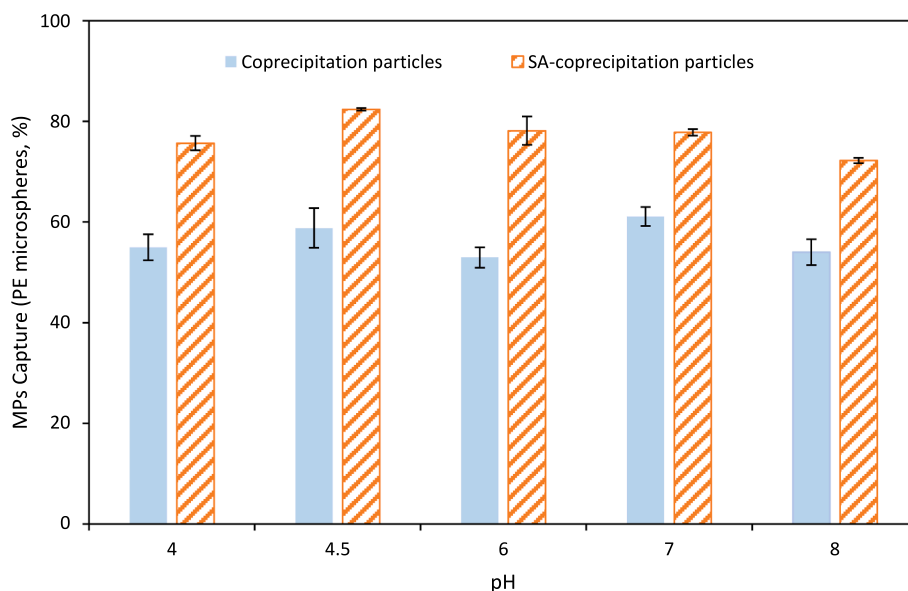


Fig. 9. PE MPs capture percentages applying SA-functionalized and bare coprecipitation particles, with pH in the range 4–8. PE MPs concentration: 0.5 g L^{-1} . Magnetic nanoparticles concentration: 1.3 g L^{-1} . Contact time: 20 min.

diameter of amino-functionalized thermal decomposition particles and non-functionalized magnetic nanoparticles are similar, which means that the addition of amino groups does not lead to an appreciable increase in size. Nonetheless, there is a visual decrease in the tendency of the amino-functionalized magnetic nanoparticles to agglomerate, which is consistent with the higher values of Z potential of the functionalized particles, which promote the stability of the particles' suspension due to repulsion phenomena.

In order to demonstrate the correct synthesis and functionalization of the different magnetic materials, Figs. S1–S4 display SEM images, EDX and elemental mapping of bare and SA-functionalized coprecipitation particles and bare and amino-functionalized thermal decomposition particles, respectively. In the EDX and elemental mapping, the synthesized magnetic materials present a strong abundance and purity of Fe ($69.1 \pm 0.5\%$) and O ($30.5 \pm 0.2\%$) as an index of the formation of the magnetic core. Moreover, Figs. S2 and S4 verify the successful surface modification of the SA-functionalized coprecipitation and amino-functionalized thermal decomposition particles due to the detection of C as consequence of the sodium alginate coating, and N and Si because of the addition of amino-based alkoxy silanes employed for functionalization.

Furthermore, Fig. 5.A shows the hysteresis loops obtained by the magnetic characterization of the different nanoparticles. A noteworthy property of the synthesized materials is the superparamagnetic behaviour, which is confirmed by the fact that all the magnetic curves show values of magnetization close to 0 when the magnetic field becomes 0 Oe (see inset of Fig. 5A) [72]. According to the magnetic saturation values, particles synthesized by thermal decomposition show a higher magnetic saturation value, of 66 emu g^{-1} , than those obtained for coprecipitation particles, 51 emu g^{-1} . This improved magnetic behaviour is attributed to the larger particle sizes presented by thermal decomposition particles, as previously depicted in Fig. 4. After the amino-functionalization and SA-functionalization of the particles synthesized by thermal decomposition and coprecipitation methods, their magnetic saturation values decreased to 63 emu g^{-1} and 49 emu g^{-1} , respectively, which does not imply a significant reduction in the superparamagnetic properties of the functionalized magnetic nanoparticles. Moreover, in Fig. 5.B, a thermogravimetric analysis is carried out to verify the surface modification of the bare magnetic nanoparticles. In the case of the non-functionalized magnetic nanoparticles, the weight loss for both the coprecipitation and thermal decomposition particles takes place in the range of $0\text{--}250 \text{ }^\circ\text{C}$

which is attributed to the water adsorbed on the surface for coprecipitation particles and the TEG coating that is produced in the synthesis method and remaining ethanol of the cleaning stage [56], respectively. In the case of functionalized magnetic nanoparticles, the weight loss in the range of $200\text{--}300 \text{ }^\circ\text{C}$ correspond to the sodium alginate coating (9.4%) for SA-coprecipitation particles [73,74], while the amino-thermal decomposition particles loss of 16.2% in the range of $250\text{--}1000 \text{ }^\circ\text{C}$ is attributed to the anchoring of amino groups [34]. In addition, the crystallographic structure of bare coprecipitation and thermal decomposition nanoparticles is confirmed in Fig. S5. Both particles share the same peak profile, which corresponds to the main phase of a crystal structure and is compatible with nanostructured compounds. The position and intensity of the diffraction peaks, match with the magnetite database in the International Centre for Diffraction Data (ICDD, PDF2: 75-0449).

3.2. Experimental analysis of MPs capture

After characterization of the magnetic nanoparticles, their viability for the capture of microplastics was tested, using polyethylene micro-particles as model pollutant. Initially, a reference experiment was performed by dispersing microplastics in water which were subjected to a magnetic field not observing any interaction.

Fig. 6 displays the percentage of microplastics captured when polyethylene microspheres were contacted with magnetic nanoparticles synthesized by thermal decomposition, for a predetermined time of 20 min. The initial concentration of PE in the suspension was 0.5 g L^{-1} while the concentration of magnetic nanoparticles ranged in the interval between 0.3 g L^{-1} and 1.8 g L^{-1} . It is observed that the capture percentage increased from $31.2 \pm 4.8\%$ to $72.8 \pm 1.1\%$ when the magnetic nanoparticles initial concentration varied from 0.3 to 1.8 g L^{-1} . However, no significant change in the capture percentage was observed after 20 min of contact time for concentrations $\geq 1.3 \text{ g L}^{-1}$. Therefore, this value was selected as the initial concentration of magnetic nanoparticles for further research. These capture results are consistent with those obtained by Shi et al. [40], who reported that the addition of a higher concentration of magnetic nanoparticles does not generate significant difference in the capture percentage of polyethylene MPs when using commercial nano- Fe_3O_4 particles with a size of $900 \text{ }\mu\text{m}$.

Fig. 7 the MPs capture percentage obtained when a suspension of 0.5 g L^{-1} of polyethylene microspheres and 1.3 g L^{-1} of magnetic

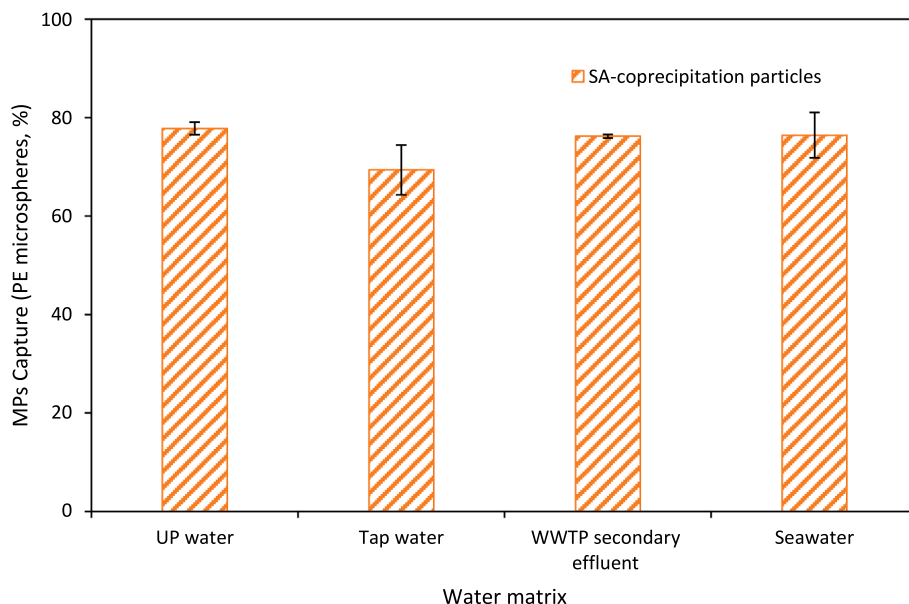


Fig. 10. PE MPs capture percentage from different water matrices applying SA-functionalized coprecipitation particles. PE MPs concentration: 0.5 g L^{-1} . Magnetic nanoparticles concentration: 1.3 g L^{-1} . Contact time: 20 min.

nanoparticles were contacted from 1 min to 240 min. Experiments were conducted for magnetic particles synthesized by thermal decomposition and by coprecipitation, to evaluate the influence of the synthesis method on the kinetics of the process.

In this work and for the experimental conditions used, it is confirmed that higher capture percentages were obtained for particles synthesized by thermal decomposition, varying from $36.6 \pm 1.5\%$ for small contact

times of 1 min to $85.3 \pm 2.9\%$ for 30 min whereas capture percentages with coprecipitation particles ranged from $22.6 \pm 3.3\%$ to $57.2 \pm 7.5\%$. However, in both cases, an increase in the contact time led to an increase in the capture percentage, achieving percentages higher than 95% for contact times of about 240 min. Therefore, the surface modification of magnetic nanoparticles improves the capture kinetics, but does not affect the maximum capture percentage. For further experiments, an

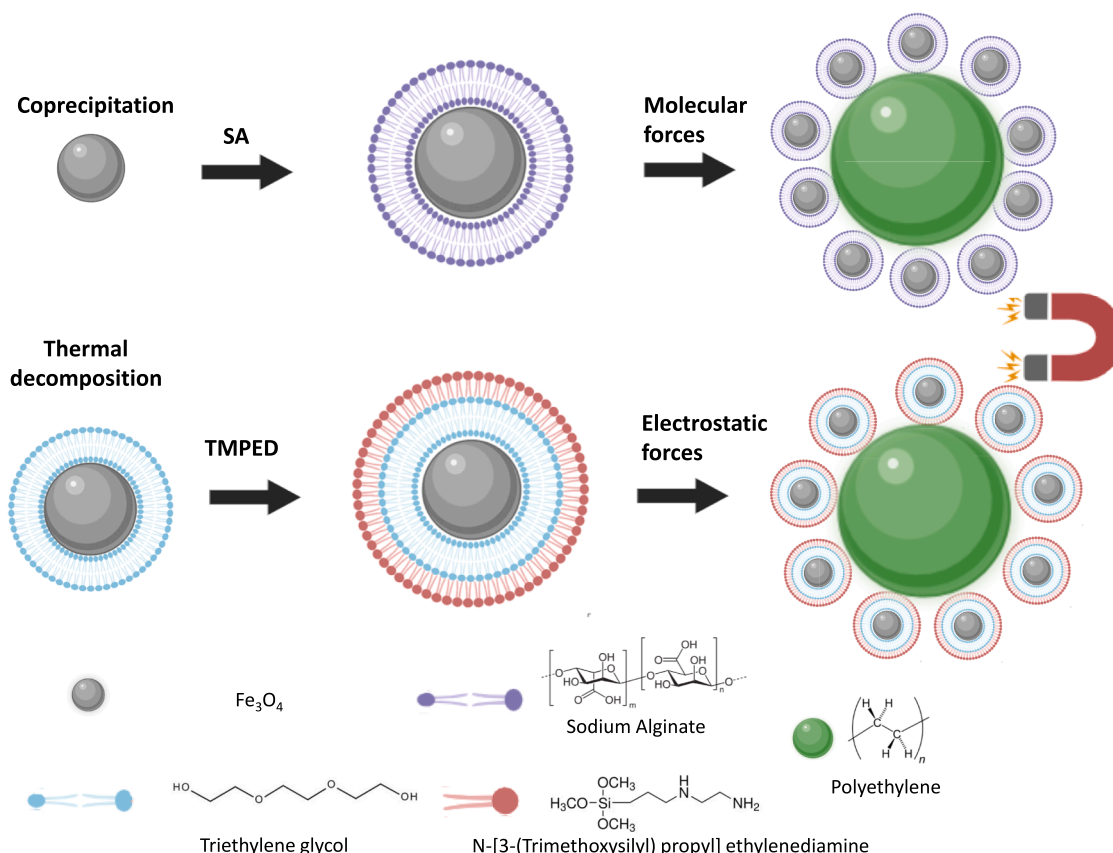


Fig. 11. Different mechanisms of the capture of polyethylene microplastics.

Table 1
Comparison of the MPs capture efficiency from other researches.

Magnetic nanoparticles	Magnetic nanoparticles Concentration (g L^{-1})	MPs	MPs size (μm)	MPs Concentration (g L^{-1})	Magnetic nanoparticles/MPs Ratio	Contact time (min)	Capture percentage (%)	Reference
Nano- Fe_3O_4	1.3	PE	900	0.5	2.6	150	98	[30]
Fe_3O_4 -PWA/nOct	1	PS	1	0.001	1000	360–720	99	[41]
Fe_3O_4 @ C_{12}	10	GFL-PS	0.2	1	10	660	90	[81]
Nano- Fe @ZIF-8	1	PS	1.1	0.025	40	5	88.7	[82]
PEG/ Fe_3O_4	2	PE	13–149	2	1	180	84	[83]
Amino-thermal decomposition particles	1.3	PE	212–250	0.5	2.6	20	75.5	This work
SA-coprecipitation particles	1.3	PE	212–250	0.5	2.6	20	82.4	This work

intermediate time of 20 min is selected as the contact time between magnetic nanoparticles and MPs, since capture percentages around 60% were obtained, high enough to appreciate changes when modifying other variables such as the synthesis method, pH or functional groups.

To evaluate the differences in the capture kinetics observed with particles synthesized by both methods, an analysis of the expected interactions between magnetic nanoparticles and MPs has been carried out. If it is initially assumed that electrostatic interaction is the main mechanism responsible for the capture of MPs, at pH 5.2 and regarding the values of zeta potential depicted in Fig. 3B, the bare coprecipitation particles would be expected to show faster capture at this pH since the difference in the surface charge of these particles and MPs is greater than the observed difference with thermal decomposition particles. Nevertheless, as better performance is achieved with thermal decomposition particles, it is concluded that electrostatic interaction may not be the main interaction mechanism in this case.

When using coprecipitation particles, as shown in Fig. 2, the water adsorption on the surface of the magnetic nanoparticles led to the presence of OH groups on their surface. The presence of these groups leads to the formation of hydrogen bonds between magnetic nanoparticles and MPs. The slightly enhanced capture of the thermal decomposition particles may be attributed to the higher contribution of hydrogen bonds formed due to the TEG coating which provides a higher number of hydroxyl groups than the water adsorbed on the particle surface [75]. Furthermore, the affinity of microplastics towards organic compounds, such as the TEG coating, has been previously confirmed in literature [25,26,76,77]. Therefore, the surface modification of magnetic nanoparticles improves the capture kinetics, not affecting the maximum capture percentage. For this reason, it is key to functionalize magnetic nanoparticles in order to achieve better results in terms of faster MPs capture.

To confirm the hypothesis that the formation of hydrogen bonds is the main interaction mechanism, the influence of pH was evaluated. Besides, the behaviour of magnetic nanoparticles functionalized with amino groups and sodium alginate was studied and compared with the performance of bare magnetite nanoparticles. Suspensions of 0.5 g L^{-1} of polyethylene MPs and 1.3 g L^{-1} of bare coprecipitation and amino-functionalized thermal decomposition nanoparticles were adjusted to different pH values in the range 5 to 8 and left inside an ultrasonic bath for 20 min; results are shown in Fig. 8. According to the values of zeta potential (Fig. 3B), bare coprecipitation particles might be active in the range of pH 4–7. The bare coprecipitation particles showed capture percentages ranging from $52.9 \pm 2.1\%$ to $61.1 \pm 1.9\%$ between pH 4 and pH 8. At pH 8 coprecipitation particles and microplastics were expected to exhibit repulsive interactions, but the capture percentage did not vary significantly compared to the values obtained at lower pH values, confirming that electrostatic forces were not the main interaction force as it was previously mentioned. Consequently, both coprecipitation and thermal decomposition particles exhibit hydrogen bonds as the main interaction force due to the hydroxyl groups of adsorbed water and TEG, respectively.

Fig. 8 also shows an increase of the capture percentage when using amino-functionalized particles compared to coprecipitation particles. In this case, amino-functionalized nanoparticles are expected to attract electrostatically negatively charged microplastics in the range pH 5–8. The results showed capture percentages that varied from $75.5 \pm 2.3\%$ at pH 5 to $48.8 \pm 1.2\%$ at pH 8. The decrease in the capture percentage of MPs with an increase in the pH value is attributed to deprotonation of amino groups on the surface of the magnetic nanoparticles that weakens their electrostatic affinity towards microplastics. Comparing these results with the performance of bare magnetic nanoparticles, it is observed that amino-functionalization improves the capture of MPs at pH 5; however, when pH increases, coprecipitation particles exhibit similar performance than functionalized nanoparticles. Consequently, functionalization of magnetic nanoparticles with amino groups makes the particles interact with MPs through electrostatic attraction as the main force.

Furthermore, coprecipitation particles, which were synthesized by a more cost-effective and greener process compared to thermal decomposition particles, were functionalized with sodium alginate. Suspensions of 0.5 g L^{-1} of polyethylene MPs and 1.3 g L^{-1} of SA-functionalized and bare coprecipitation magnetic nanoparticles were adjusted to different pH values in the range 4–8 and left stirring for 20 min; results are shown in Fig. 9. This figure shows an increase of the capture percentage when using SA-functionalized particles compared to the non-functionalized coprecipitation particles with values ranging from $72.2 \pm 0.5\%$ to $82.4 \pm 0.3\%$ corresponding to SA-coprecipitation particles. Additionally, outside the attraction zone depicted in Fig. 3C, the capture percentage decreased when the zeta potential values of magnetic nanoparticles became more negative with values of $76.1 \pm 2.8\%$, $75.8 \pm 0.6\%$ and $72.2 \pm 0.5\%$ at pH 6, 7 and 8, respectively. However, the variation was not very significant, indicating that electrostatic interactions are not the predominant mechanism.

As previously mentioned, bare coprecipitation particles and MPs exhibit hydrogen bonds due to the hydroxyl groups. However, when using SA-functionalized particles, an increase in the capture percentage is observed compared to bare coprecipitation particles. This increase in the capture percentage was attributed to the presence of polar groups such as COOH and OH in sodium alginate molecules, which contributed to the formation of hydrogen bonds. As reported by Rafa et al. [78], Ma et al. [79] and He et al. [80], microplastics have the ability to form hydrogen bonds with polar functional groups, thereby enhancing their adhesion and transport in different media. Therefore, the surface-modified coprecipitation particles exhibited strong interactions with PE microparticles, thereby improving the capture kinetics.

Comparing the capture percentage of MPs by using amino and sodium alginate surface-modified magnetic nanoparticles, the alginate-functionalization reported the highest values, which is consistent with the appearance of hydrogen bonds as the main interaction mechanism. Furthermore, the cost-effective, fast and greener synthesis and functionalization process of these SA-functionalized particles is a remarkable novelty for the removal of MPs in wastewater.

Finally, the analysis of the influence of the water matrix on the removal of microplastics was carried out. Ultrapure water, tap water, seawater and WWTP secondary effluent were used as water matrices with pH values of ≈ 7.00 , 7.99 ± 0.04 , 8.13 ± 0.01 and 7.14 ± 0.44 , respectively. SA-functionalized magnetic nanoparticles were selected for the removal of microplastics due to the fastest capture results and the independence of the pH values on the separation. Suspensions of 0.5 g L^{-1} of polyethylene MPs and 1.3 g L^{-1} of SA-functionalized coprecipitation nanoparticles were prepared using different water matrices and left inside an ultrasonic bath for 20 min. Fig. 10 displays the results of the microplastics capture percentages when using different matrices. Due to the small differences in the capture percentage, the influence of the water matrix on the removal of microplastics is considered negligible, confirming the formation of hydrogen bonds, which are independent of the pH. Therefore, the presence of wastewater constituents, such as monovalent or divalent salts and natural organic matter, does not contribute to a worse performance in the capture method, which implies a noteworthy contribution to be applied in advanced water treatment processes.

Fig. 11 summarizes the mechanisms responsible for the capture of polyethylene microplastics by using surface-modified magnetic nanoparticles. The coprecipitation synthesis method gives rise to bare magnetite particles, while the thermal decomposition method leads to particles that exhibit a coating due to the use of triethylene glycol as surfactant during the synthesis. The SA-functionalization of the coprecipitation particles causes the magnetic nanoparticles to interact with the MPs through hydrogen bonding as the main force and the interaction of the amino-functionalized thermal decomposition particles is related to electrostatic forces. According to the surface interactions, the particles with polar groups on their surface interact with MPs through electrostatic interactions or hydrogen bonds (depending on the type of the groups).

As shown in Table 1, a wide range of MPs removal percentages have been reported in the literature which are strongly affected by several variables such as the contact time, the mass ratio between the magnetic nanoparticles and MPs, and the particle size. The main novelty of this work is associated with the evaluation of the mechanisms of MPs capture when using different functionalized magnetic nanoparticles. Moreover, the effectiveness of the surface modified magnetic nanoparticles in this research is promising since SA-coprecipitation particles exhibit a remarkably high capture efficiency of PE MPs with relatively slow contact times compared with bibliography. Besides, the results obtained prove the applicability of these functional nanoparticles for the capture of PE MPs from polluted waters under different pH conditions, i.e. groundwaters usually exhibit pH values around 6, whereas river waters and seawaters have pH values of 7.4 and 8, respectively [69–71].

4. Conclusions

This work proposes the use of magnetic nanoparticles, for the fast, cost-effective and environmentally friendly capture of microplastic pollutants in aqueous sources. Magnetic nanoparticles were obtained following two synthesis methods: the coprecipitation method and the thermal decomposition method, and the capture of polyethylene microplastics $232 \pm 8 \mu\text{m}$ from a 0.5 g L^{-1} suspension was selected as representative case of study. First, an increase in the initial concentration of magnetic nanoparticles synthesized by thermal decomposition, resulted in an increase in the capture percentage of microplastics. Nevertheless, no significant change was observed after 20 min of contact time for magnetic particles concentrations $\geq 1.3 \text{ g L}^{-1}$, considered the optimum value to achieve the maximum polyethylene capture. Furthermore, after 20 min of contact time, particles synthesized by batch thermal decomposition captured $69.3 \pm 2.1\%$ of the PE MPs, a value higher than the $57.2 \pm 7.5\%$ showed by coprecipitation particles. This improved behaviour was attributed to the TEG coating that is formed around the magnetic core during the thermal decomposition

synthesis, which provides polar groups that enhance its intermolecular interactions toward MPs.

The surface modification was also evaluated to analyze the enhanced interactions of the amino-functionalized thermal decomposition and SA-functionalized coprecipitation particles with the MPs. The anchoring of amino groups on the surface of the magnetic nanoparticles led to a significant increase in the zeta potential values and, consequently, to a shift of their isoelectric point to higher pH values moving from pH 6 to pH 8. Moreover, a capture percentage of $75.5 \pm 2.3\%$ was obtained at pH 5 but it decreased with the increase in zeta potential values due to repulsion electrostatic forces. The SA coating in the coprecipitation particles reduced the zeta potential values and the isoelectric point and weakened electrostatic forces towards MPs. However, capture percentages ranging from $82.4 \pm 0.3\%$ at pH 4.5 to $72.2 \pm 0.5\%$ at pH 8 were achieved, which were higher than those of the amino-functionalized particles. This improvement was attributed to the contribution of carboxyl and hydroxyl groups to the formation of hydrogen bonds. Furthermore, the MPs capture percentage did not vary when changing the water matrix to a polluted water source. Overall, the methodology reported in this work represents a step forward in the development of new reliable technologies for the removal of microplastics from aqueous sources and can be extended to different water sources including groundwater (pH 6), rivers (pH 7.4) and seawater (pH 8).

As future work, considering the best experimental conditions obtained in this research work, the regeneration and reusability of the functionalized magnetic nanoparticles will be evaluated. For this purpose, the addition of surfactants and the modification of pH of the media will be carried out to recycle the magnetic nanoparticles which are adhered to the MPs and analyze the capture performance after several experiments, contributing to a more sustainable approach for environmental applications. Besides, it is also planned to study the possible degradation of the separated microplastics using magnetic-based photocatalytic materials, avoiding any additional waste generation. Moreover, an upcoming challenge is transferring the knowledge acquired in these batch capture experiments to a continuous mode, following the insights of the same research group that has already worked in microfluidic devices for the continuous capture of pollutants using magnetic nanoparticles and their subsequent magnetophoretic separation. Finally, the molecular interactions will be analyzed using a molecular dynamic simulation software. Before the simulation of the interactions, a modeling of the magnetic nanoparticles and the microplastics has to be made, trying to minimize the computational load and time consumption.

Declaration of competing interest

The authors declare that they have no known competing financial interests or personal relationships that could have appeared to influence the work reported in this paper.

Data availability

The data that has been used is confidential.

Acknowledgements

These results are part of the R&D project PID2021-122563OB-I00 funded by MICIU/AEI/10.13039/501100011033 and by “ERDF/EU”. Daniel Aragón is grateful for the grant PRE2022-104908 funded by MICIU/AEI/10.13039/501100011033 and by “ESF+”. Belén García-Merino is grateful for the grant PRE2019-089339 and funded by MICIU/AEI/10.13039/501100011033 and by “ESF Investing in your future”. Carmen Barquín is grateful for the grant PRE2019-089096 and funded by MICIU/AEI/10.13039/501100011033 and by “ESF Investing in your future”. Authors also thanks the technical and human support provided by materials characterization service (SERCAMAT) of the University of Cantabria and the microscopy unit of the Health Research Institute

IDIVAL.

Appendix A. Supplementary data

Supplementary data to this article can be found online at <https://doi.org/10.1016/j.seppur.2024.128813>.

References

- [1] G. Bonifazi, L. Fiore, C. Pelosi, S. Serranti, Evaluation of plastic packaging waste degradation in seawater and simulated solar radiation by spectroscopic techniques, *Polym. Degrad. Stab.* 207 (2023) 1–16, <https://doi.org/10.1016/j.polydegradstab.2022.110215>.
- [2] Plastics Europe AISBL, *Plastics - the fast Facts 2023*, (2023).
- [3] R.C. Thompson, Y. Olsen, R.P. Mitchell, A. Davis, S.J. Rowland, A.W.G. John, D. McGonigle, A.E. Russell, Lost at sea: where is all the plastic? *Science* 304 (2004) 838, <https://doi.org/10.1126/science.1094559>.
- [4] M. Yan, H. Nie, K. Xu, Y. He, Y. Hu, Y. Huang, J. Wang, Microplastic abundance, distribution and composition in the Pearl River along Guangzhou city and Pearl River estuary, China, *Chemosphere* 217 (2019) 879–886, <https://doi.org/10.1016/j.chemosphere.2018.11.093>.
- [5] W. Courteney-Jones, B. Quinn, S.F. Gary, A.O.M. Mogg, B.E. Narayanaswamy, Microplastic pollution identified in deep-sea water and ingested by benthic invertebrates in the Rockall Trough, North Atlantic Ocean, *Environ. Pollut.* 231 (2017) 271–280, <https://doi.org/10.1016/j.envpol.2017.08.026>.
- [6] J.H. Fernández, H. Cano, Y. Guerra, E.P. Polo, J.F. Ríos-Rojas, R. Vivas-Reyes, J. Oviedo, Identification and quantification of microplastics in effluents of wastewater treatment plant by differential scanning calorimetry (DSC), *Sustainability (switzerland)* 14 (2022), <https://doi.org/10.3390/su14094920>.
- [7] A. Tirkey, L.S.B. Upadhyay, Microplastics: an overview on separation, identification and characterization of microplastics, *Mar. Pollut. Bull.* 170 (2021) 1–12, <https://doi.org/10.1016/j.marpolbul.2021.112604>.
- [8] M.N. Issac, B. Kandasubramanian, Effect of microplastics in water and aquatic systems, *Environ. Sci. Pollut. Res.* 28 (2021) 19544–19562, <https://doi.org/10.1007/s11356-022-13184-2>.
- [9] K. Ugwu, A. Herrera, M. Gómez, Microplastics in marine biota: a review, *Mar. Pollut. Bull.* 169 (2021) 1–11, <https://doi.org/10.1016/j.marpolbul.2021.112540>.
- [10] M.S.L. Yee, L.W. Hii, C.K. Looi, W.M. Lim, S.F. Wong, Y.Y. Kok, B.K. Tan, C. Y. Wong, C.O. Leong, Impact of microplastics and nanoplastics on human health, *Nanomaterials* 11 (2021) 1–23, <https://doi.org/10.3390/nano11020496>.
- [11] N. Porcino, T. Bottari, M. Mancuso, Is wild marine biota affected by microplastics? *Animals* 13 (2023) 1–17, <https://doi.org/10.3390/ani13010147>.
- [12] O. Bajt, From plastics to microplastics and organisms, *FEBS Open Bio* 11 (2021) 954–966, <https://doi.org/10.1002/2211-5463.13120>.
- [13] H. Du, Y. Xie, J. Wang, Microplastic degradation methods and corresponding degradation mechanism: research status and future perspectives, *J. Hazard. Mater.* 418 (2021) 1–8, <https://doi.org/10.1016/j.jhazmat.2021.126377>.
- [14] D. la Cecilia, M. Philipp, R. Kaegi, M. Schirmer, C. Moeck, Microplastics attenuation from surface water to drinking water: impact of treatment and managed aquifer recharge – and identification uncertainties, *Sci. Total Environ.* 908 (2024), <https://doi.org/10.1016/j.scitotenv.2023.168378>.
- [15] Y. Lu, M.C. Li, J. Lee, C. Liu, C. Mei, Microplastic remediation technologies in water and wastewater treatment processes: current status and future perspectives, *Sci. Total Environ.* 868 (2023), <https://doi.org/10.1016/j.scitotenv.2023.161618>.
- [16] O.M. Rodríguez-Narvaez, A. Goonetilleke, L. Perez, E.R. Bandala, Engineered technologies for the separation and degradation of microplastics in water: a review, *Chem. Eng. J.* 414 (2021) 1–13, <https://doi.org/10.1016/j.cej.2021.128692>.
- [17] W. Hamd, E.A. Daher, T.S. Tofa, J. Dutta, Recent advances in photocatalytic removal of microplastics: mechanisms, kinetic degradation, and reactor design, *Front. Mar. Sci.* 9 (2022) 1–28, <https://doi.org/10.3389/fmars.2022.885614>.
- [18] S. Kim, Y. Hyeon, H. Rho, C. Park, Ceramic membranes as a potential high-performance alternative to microplastic filters for household washing machines, *Sep. Purif. Technol.* 344 (2024), <https://doi.org/10.1016/j.seppur.2024.127278>.
- [19] I. Ali, T. Ding, C. Peng, I. Naz, H. Sun, J. Li, J. Liu, Micro- and nanoplastics in wastewater treatment plants: Occurrence, removal, fate, impacts and remediation technologies – A critical review, *Chem. Eng. J.* 423 (2021), <https://doi.org/10.1016/j.cej.2021.130205>.
- [20] I. Ali, T. Ding, C. Peng, I. Naz, H. Sun, J. Li, J. Liu, Micro- and nanoplastics in wastewater treatment plants: occurrence, removal, fate, impacts and remediation technologies – A critical review, *Chem. Eng. J.* 423 (2021) 1–35, <https://doi.org/10.1016/j.cej.2021.130205>.
- [21] N. Morin-Crini, E. Lichtfouse, M. Fourmentin, A.R.L. Ribeiro, C. Noutsopoulos, F. Mapelli, É. Fenyvesi, M.G.A. Vieira, L.A. Picos-Corralles, J.C. Moreno-Piraján, L. Giraldo, T. Sohadja, M.M. Huq, J. Soltan, M. Maguereanu, C. Bradu, G. Crini, Removal of emerging contaminants from wastewater using advanced treatments. A review, *Environ. Chem. Lett.* 20 (2022) 1333–1375, <https://doi.org/10.1007/s10311-021-01379-5>.
- [22] B. Pandey, J. Pathak, P. Singh, R. Kumar, A. Kumar, S. Kaushik, T.K. Thakur, Microplastics in the ecosystem: an overview on detection, removal, toxicity assessment, and control release, *Water* 15 (2023) 1–31, <https://doi.org/10.3390/w15010051>.
- [23] A.D. Vital-Grappin, M.C. Ariza-Tarazona, V.M. Luna-Hernández, J.F. Villarreal-Chiu, J.M. Hernández-López, C. Siligardi, E.I. Cedillo-González, The role of the reactive species involved in the photocatalytic degradation of hdpe microplastics using C, N-TiO₂ powders, *Polymers (basel)* 13 (2021), <https://doi.org/10.3390/polym13070999>.
- [24] Y. Cao, C.I. Sathish, X. Guan, S. Wang, T. Palanisami, A. Vinu, J. Yi, Advances in magnetic materials for microplastic separation and degradation, *J. Hazard. Mater.* 461 (2024), <https://doi.org/10.1016/j.jhazmat.2023.132537>.
- [25] Y. Yu, W.Y. Mo, T. Luukkonen, Adsorption behaviour and interaction of organic micropollutants with nano and microplastics – A review, *Sci. Total Environ.* 797 (2021) 1–11, <https://doi.org/10.1016/j.scitotenv.2021.149140>.
- [26] Y. Sun, J. Ji, J. Tao, Y. Yang, D. Wu, L. Han, S. Li, J. Wang, Current advances in interactions between microplastics and dissolved organic matters in aquatic and terrestrial ecosystems, *TrAC – Trends Anal. Chem.* 158 (2023) 1–14, <https://doi.org/10.1016/j.trac.2022.116882>.
- [27] L. Fu, J. Li, G. Wang, Y. Luan, W. Dai, Adsorption behavior of organic pollutants on microplastics, *Ecotoxicol. Environ. Saf.* 217 (2021) 112207, <https://doi.org/10.1016/j.ecoenv.2021.112207>.
- [28] S. He, Y. Wei, C. Yang, Z. He, Interactions of microplastics and soil pollutants in soil-plant systems, *Environ. Pollut.* 315 (2022) 120357, <https://doi.org/10.1016/j.envpol.2022.120357>.
- [29] V. Kinigopoulou, I. Pashalidis, D. Kalderis, I. Anastopoulos, Microplastics as carriers of inorganic and organic contaminants in the environment: a review of recent progress, *J. Mol. Liq.* 350 (2022) 118580, <https://doi.org/10.1016/j.molliq.2022.118580>.
- [30] C. Shi, S. Zhang, J. Zhao, J. Ma, H. Wu, H. Sun, S. Cheng, Experimental study on removal of microplastics from aqueous solution by magnetic force effect on the magnetic separation, *Sep. Purif. Technol.* 288 (2022), <https://doi.org/10.1016/j.seppur.2022.120564>.
- [31] L. Wu, A. Mendoza-Garcia, Q. Li, S. Sun, Organic phase syntheses of magnetic nanoparticles and their applications, *Chem. Rev.* 116 (2016) 10473–10512, <https://doi.org/10.1021/acs.chemrev.5b00687>.
- [32] B. García-Merino, E. Bringas, I. Ortiz, Synthesis and applications of surface-modified magnetic nanoparticles: Progress and future prospects, *Rev. Chem. Eng.* 38 (2021) 821–842, <https://doi.org/10.1515/revce-2020-0072>.
- [33] J. Gómez-Pastora, X. Xue, I.H. Karampelas, E. Bringas, E.P. Furlani, I. Ortiz, Analysis of separators for magnetic beads recovery: From large systems to multifunctional microdevices, *Sep. Purif. Technol.* 172 (2017) 16–31, <https://doi.org/10.1016/j.seppur.2016.07.050>.
- [34] B. García-Merino, E. Bringas, I. Ortiz, Robust system for the regenerative capture of aqueous pollutants with continuously synthesized and functionalized magnetic nanoparticles, *J. Environ. Chem. Eng.* 10 (2022) 1–13, <https://doi.org/10.1016/j.jece.2022.108417>.
- [35] J. Saiz, E. Bringas, I. Ortiz, New functionalized magnetic materials for As⁵⁺ removal: adsorbent regeneration and reuse, *Ind. Eng. Chem. Res.* 53 (2014) 18928–18934, <https://doi.org/10.1021/ie500912k>.
- [36] G. Liu, L. Liao, Z. Dai, Q. Qi, J. Wu, L.Q. Ma, C. Tang, J. Xu, Organic adsorbents modified with citric acid and Fe₃O₄ enhance the removal of Cd and Pb in contaminated solutions, *Chem. Eng. J.* 395 (2020), <https://doi.org/10.1016/j.cej.2020.125108>.
- [37] S. Shi, C. Xu, X. Wang, Y. Xie, Y. Wang, Q. Dong, L. Zhu, G. Zhang, D. Xu, Electrospinning fabrication of flexible Fe₃O₄ fibers by sol-gel method with high saturation magnetization for heavy metal adsorption, *Mater. Des.* 186 (2020), <https://doi.org/10.1016/j.matdes.2019.108298>.
- [38] J. Grbic, B. Nguyen, E. Guo, J.B. You, D. Sinton, C.M. Rochman, Magnetic extraction of microplastics from environmental samples, *Environ. Sci. Technol. Lett.* 6 (2019) 68–72, <https://doi.org/10.1021/acs.estlett.8b00671>.
- [39] A. Misra, C. Zambrycki, G. Kloker, A. Kotyrbá, M.H. Anjass, I. Franco Castillo, S. G. Mitchell, R. Güttel, C. Streb, Water purification and microplastics removal using magnetic polyoxometalate-supported ionic liquid phases (magPOM-SILPs), *Angew. Chem.* 59 (2020) 1601–1605, <https://doi.org/10.1002/anie.201912111>.
- [40] X. Shi, X. Zhang, W. Gao, Y. Zhang, D. He, Removal of microplastics from water by magnetic nano-Fe₃O₄, *Sci. Total Environ.* 802 (2022) 1–8, <https://doi.org/10.1016/j.scitotenv.2021.149838>.
- [41] R.K. Bhole, S.B. Kamble, Nano adsorptive extraction of diverse microplastics from the potable and seawater using organo-polyoxometalate magnetic nanocomposites, *J. Environ. Chem. Eng.* 10 (2022), <https://doi.org/10.1016/j.jece.2022.108720>.
- [42] L.M.A. Martin, J. Sheng, P.V. Zimba, L. Zhu, O.O. Fadare, C. Haley, M. Wang, T. D. Phillips, J. Conkle, W. Xu, Testing an iron oxide nanoparticle-based method for magnetic separation of nanoplastics and microplastics from water, *Nanomaterials* 12 (2022), <https://doi.org/10.3390/nano12142348>.
- [43] A. Tomitaka, A. Kaushik, B.D. Kevaliyaj, I. Mukadam, H.E. Gendelman, K. Khalili, G. Liu, M. Nair, Surface-engineered multimodal magnetic nanoparticles to manage CNS diseases, *Drug Discov. Today* 24 (2019) 873–882, <https://doi.org/10.1016/j.drudis.2019.01.006>.
- [44] S.S. Sadri, R.C. Thompson, On the quantity and composition of floating plastic debris entering and leaving the Tamar Estuary, Southwest England, *Mar. Pollut. Bull.* 81 (2014) 55–60, <https://doi.org/10.1016/j.marpolbul.2014.02.020>.
- [45] S.M. Mintenig, I. Int-Veen, M.G.J. Löder, S. Primpke, G. Gerds, Identification of microplastic in effluents of waste water treatment plants using focal plane array-based micro-Fourier-transform infrared imaging, *Water Res.* 108 (2017) 365–372, <https://doi.org/10.1016/j.watres.2016.11.015>.
- [46] M. Ghanadi, I. Joshi, N. Dharmasiri, J.E. Jaeger, M. Burke, C. Bebelman, B. Symons, L.P. Padhye, Quantification and characterization of microplastics in coastal environments: Insights from laser direct infrared imaging, *Sci. Total Environ.* 912 (2024), <https://doi.org/10.1016/j.scitotenv.2023.168835>.

- [47] A. Hurtado, A.A.A. Aljabali, V. Mishra, M.M. Tambuwala, Á. Serrano-Aroca, Alginate: enhancement strategies for advanced applications, *Int. J. Mol. Sci.* 23 (2022), <https://doi.org/10.3390/ijms23094486>.
- [48] M.J. Molaie, E. Salimi, Magneto-fluorescent superparamagnetic Fe₃O₄@SiO₂@alginate/carbon quantum dots nanohybrid for drug delivery, *Mater. Chem. Phys.* 288 (2022), <https://doi.org/10.1016/j.matchemphys.2022.126361>.
- [49] O.A.A. El-Shamy, R.E. El-Azabawy, O.E. El-Azabawy, Synthesis and characterization of magnetite-alginate nanoparticles for enhancement of nickel and cobalt ion adsorption from wastewater, *J. Nanomater.* 2019 (2019), <https://doi.org/10.1155/2019/6326012>.
- [50] A. K ppler, F. Windrich, M.G.J. L der, M. Malanin, D. Fischer, M. Labrenz, K. J. Eichhorn, B. Voit, Identification of microplastics by FTIR and Raman microscopy: a novel silicon filter substrate opens the important spectral range below 1300 cm⁻¹ for FTIR transmission measurements, *Anal. Bioanal. Chem.* 407 (2015) 6791–6801, <https://doi.org/10.1007/s00216-015-8850-8>.
- [51] J.X. Wong, S.N. Gan, M.J. Aishah, Chromium(III) based ziegler-natta catalysts for olefin polymerization, *Sains Malays.* 40 (2011) 771–779.
- [52] C. Barqu n, M.J. Rivero, I. Ortiz, Shedding light on the performance of magnetically recoverable TiO₂/Fe₃O₄/rGO-5 photocatalyst. Degradation of S-metolachlor as case study, *Chemosphere* 307 (2022) 135991, <https://doi.org/10.1016/j.chemosphere.2022.135991>.
- [53] R. Fattahi Nafchi, R. Ahmadi, M. Heydari, M.R. Rahimpour, M.J. Molaie, L. Unsworth, In vitro study: synthesis and evaluation of Fe₃O₄/CQD magnetic/fluorescent nanocomposites for targeted drug delivery, MRI, and cancer cell labeling applications, *Langmuir* 38 (2022) 3804–3816, <https://doi.org/10.1021/acs.langmuir.1c03458>.
- [54] W. Cai, J. Wan, Facile synthesis of superparamagnetic magnetite nanoparticles in liquid polyols, *J. Colloid Interface Sci.* 305 (2007) 366–370, <https://doi.org/10.1016/j.jcis.2006.10.023>.
- [55] D. Maity, P. Chandrasekharan, C.T. Yang, K.H. Chuang, B. Shuter, J.M. Xue, J. Ding, S.S. Feng, Facile synthesis of water-stable magnetite nanoparticles for clinical MRI and magnetic hyperthermia applications, *Nanomedicine* 5 (2010) 1571–1584, <https://doi.org/10.2217/nmm.10.77>.
- [56] J.K. Sahoo, S.K. Paikra, M. Mishra, H. Sahoo, Amine functionalized magnetic iron oxide nanoparticles: Synthesis, antibacterial activity and rapid removal of Congo red dye, *J. Mol. Liq.* 282 (2019) 428–440, <https://doi.org/10.1016/j.molliq.2019.03.033>.
- [57] J. Saiz, E. Bringas, I. Ortiz, Functionalized magnetic nanoparticles as new adsorption materials for arsenic removal from polluted waters, *J. Chem. Technol. Biotechnol.* 89 (2014) 909–918, <https://doi.org/10.1002/jctb.4331>.
- [58] Z. Mokadem, S. Mekki, S. Sa di-Besbes, G. Agusti, A. Elaissari, A. Derroud, Triazole containing magnetic core-silica shell nanoparticles for Pb²⁺, Cu²⁺ and Zn²⁺ removal, *Arab. J. Chem.* 10 (2017) 1039–1051, <https://doi.org/10.1016/j.arabj.2016.12.008>.
- [59] R.A. Bini, R.F.C. Marques, F.J. Santos, J.A. Chaker, M. Jafellicci, Synthesis and functionalization of magnetite nanoparticles with different amino-functional alkoxy silanes, *J. Magn. Magn. Mater.* 324 (2012) 534–539, <https://doi.org/10.1016/j.jmmm.2011.08.035>.
- [60] B. Garc a-Merino, E. Bringas, I. Ortiz, Fast and reliable analysis of pH-responsive nanocarriers for drug delivery using microfluidic tools, *Int. J. Pharm.* 643 (2023), <https://doi.org/10.1016/j.ijpharm.2023.123232>.
- [61] Malvern Ltd., Zeta potential: An Introduction in 30 minutes. Zetasizer Nano Series Tech. Note. MRK654-01 2 (2011) 1–6.
- [62] P.M.V. Raja, A.R. Barron, Physical methods in chemistry, *Nature* 134 (1934) 366–367, <https://doi.org/10.1002/jctb.5000533702>.
- [63] Q. Mo, X. Yang, J. Wang, H. Xu, W. Li, Q. Fan, S. Gao, W. Yang, C. Gao, D. Liao, Y. Li, Y. Zhang, Adsorption mechanism of two pesticides on polyethylene and polypropylene microplastics: DFT calculations and particle size effects, *Environ. Pollut.* 291 (2021) 1–9, <https://doi.org/10.1016/j.envpol.2021.118120>.
- [64] T. Xu, R. Fu, L. Yan, A new insight into the adsorption of bovine serum albumin onto porous polyethylene membrane by zeta potential measurements, FTIR analyses, and AFM observations, *J. Colloid Interface Sci.* 262 (2003) 342–350, [https://doi.org/10.1016/S0021-9797\(03\)00208-X](https://doi.org/10.1016/S0021-9797(03)00208-X).
- [65] M.H. Jang, M.S. Kim, M. Han, D.H. Kwak, Experimental application of a zero-point charge based on pH as a simple indicator of microplastic particle aggregation, *Chemosphere* 299 (2022), <https://doi.org/10.1016/j.chemosphere.2022.134388>.
- [66] K. Hayashi, H. Tomonaga, T. Matsuyama, J. Ida, Facile synthesis, characterization of various polymer immobilized on magnetite nanoparticles applying the coprecipitation method, *J. Appl. Polym. Sci.* 139 (2022), <https://doi.org/10.1002/app.51581>.
- [67] A.Z.M. Badruddoza, Z.B.Z. Shawon, M.T. Rahman, K.W. Hao, K. Hidajat, M. S. Uddin, Ionically modified magnetic nanomaterials for arsenic and chromium removal from water, *Chem. Eng. J.* 225 (2013) 607–615, <https://doi.org/10.1016/j.cej.2013.03.114>.
- [68] Y. Liu, Z. Jin, H. Meng, X. Zhang, Study on the enhanced adsorption properties of lysozyme on polyacrylic acid modified TiO₂ nano-adsorbents, *Mater. Res. Express* 5 (2018), <https://doi.org/10.1088/2053-1591/aaa169>.
- [69] M.M. Atabaki, Y.K. Siong, J. Idris, M.M. Atabaki, Performance of activated carbon in water filters, *Water Resour.* 1–19 (2013).
- [70] A. Srivastava, A. Cano, Analysis and forecasting of rivers pH level using deep learning, *Prog. Artif. Intell.* 11 (2022) 181–191, <https://doi.org/10.1007/s13748-021-00270-2>.
- [71] K. Kulthanan, P. Nuchkull, S. Varothai, The pH of water from various sources: an overview for recommendation for patients with atopic dermatitis, *Asia Pac. Allergy* 3 (2013) 155–160, <https://doi.org/10.5415/apallergy.2013.3.3.155>.
- [72] V. Marghussian, Magnetic Properties of Nano-Glass Ceramics, in: *Nano-Glass Ceramics*, Elsevier, 2015: pp. 181–223. <https://doi.org/10.1016/b978-0-323-35386-1.00004-9>.
- [73] S. Reddy Obireddy, S. Bellala, M. Chintha, A. Sake, S. Marata Chinna Subbarao, W. F. Lai, Synthesis and properties of alginate-based nanoparticles incorporated with different inorganic nanoparticulate modifiers for enhanced encapsulation and controlled release of favipiravir, *Arabian J. Chem.* 16 (2023). <https://doi.org/10.1016/j.arabj.2023.104751>.
- [74] U. Bimendra Gunatilake, M. Venkatesan, L. Basabe-Desmots, F. Benito-Lopez, Ex situ and in situ magnetic phase synthesised magneto-driven alginate beads, *J. Colloid Interface Sci.* 610 (2022) 741–750, <https://doi.org/10.1016/j.jcis.2021.11.119>.
- [75] M. Zandieh, J. Liu, Removal and degradation of microplastics using the magnetic and nanozyme activities of bare iron oxide nanoaggregates, *Angew. Chem. Int. Ed.* 61 (2022), <https://doi.org/10.1002/anie.202212013>.
- [76] W. Mei, G. Chen, J. Bao, M. Song, Y. Li, C. Luo, Interactions between microplastics and organic compounds in aquatic environments: a mini review, *Sci. Total Environ.* 736 (2020) 1–9, <https://doi.org/10.1016/j.scitotenv.2020.139472>.
- [77] J. Wang, C. Sun, Q.X. Huang, Y. Chi, J.H. Yan, Adsorption and thermal degradation of microplastics from aqueous solutions by Mg/Zn modified magnetic biochars, *J. Hazard. Mater.* 419 (2021) 1–13, <https://doi.org/10.1016/j.jhazmat.2021.126486>.
- [78] N. Rafa, B. Ahmed, F. Zohora, J. Bakya, S. Ahmed, S.F. Ahmed, M. Mofijur, A. A. Chowdhury, F. Almomani, Microplastics as carriers of toxic pollutants: source, transport, and toxicological effects, *Environ. Pollut.* 343 (2024) 123190, <https://doi.org/10.1016/j.envpol.2023.123190>.
- [79] R. Ma, Y. Feng, J. Yu, X. Zhao, Y. Du, X. Zhang, Ultralight sponge made from sodium alginate with processability and stability for efficient removal of microplastics, *Environ. Sci. Pollut. Res.* (2023), <https://doi.org/10.1007/s11356-023-29740-x>.
- [80] S. He, Y. Wei, Z. Li, C. Yang, Aging microplastic aggravates the pollution of heavy metals in rhizosphere biofilms, *Sci. Total Environ.* 890 (2023), <https://doi.org/10.1016/j.scitotenv.2023.164177>.
- [81] H.P. Wang, X.H. Huang, J.N. Chen, M. Dong, C.Z. Nie, L. Qin, Modified superhydrophobic magnetic Fe₃O₄ nanoparticles for removal of microplastics in liquid foods, *Chem. Eng. J.* 476 (2023), <https://doi.org/10.1016/j.cej.2023.146562>.
- [82] F. Pasanen, R.O. Fuller, F. Maya, Fast and simultaneous removal of microplastics and plastic-derived endocrine disruptors using a magnetic ZIF-8 nanocomposite, *Chem. Eng. J.* 455 (2023), <https://doi.org/10.1016/j.cej.2022.140405>.
- [83] Y. Zhang, J. Duan, R. Liu, E. Petropoulos, Y. Feng, L. Xue, L. Yang, S. He, Efficient magnetic capture of PE microplastic from water by PEG modified Fe₃O₄ nanoparticles: performance, kinetics, isotherms and influence factors, *J. Environ. Sci. (China)* 147 (2024) 677–687, <https://doi.org/10.1016/j.jes.2023.07.025>.